However, KD of anti-human ADC was still high for cancer cell targeting treatment. Also, the internalization ability of the anti-TF mAbs was evident. Regarding the linker construction, the val-cit linker has been reported to be stable in human and mouse plasma and cleaved efficiently by cathepsin B in acidic conditions, such as inside the lysosome of cells.[23] Similar to the previous study, the linker constructed by us was stable under physiological conditions and cleaved by cathepsin B in an acidic condition. Also, PEG_{12} was used for stealth effect to escape from the reticuloendothelial system of the liver and spleen. Lastly, MMAE, which was chosen as the payload in this study, could suppress cell growth *via* inhibition of microtubulin. The effective concentration of this drug for the inhibition of cancer cell growth was less than 1 nM, which means that an unrealistically amount of the ADC is not necessary for the treatment.[24] The actual values of the IC_{50} of MMAE in the four pancreatic cancer cell lines were ranged from 0.97 nM to 1.16 nM. Although the IC_{50} of MMAE in these four pancreatic cancer cell lines were almost same, the low TF-expressing cells (Capan-1 and Panc-1) were more resistant to the anti-human ADC compared with the high TF-expressing cells (BxPC-3). This result indicated that TF expression levels should be analyzed before the application of the ADC.

The size of the ADC was approximately 10 nm which was almost equal to the size of mAb. High molecular weight drugs that range from 10 nm to 1,000 nm in size can use passive targeting *via* the EPR effect.[21] Indeed, the anti-human ADC can extravasate from tumor vessels, reaching through the cancer stromal barrier to periphery of the tumor tissues, and can be retained up to 1 week by active targeting. Likely due to the high affinity of the ADC for tumor tissues, anti-human ADC that reached the periphery of the tumor lesion became trapped in the outer regions of the tumor and could not penetrate into the center of tumor lesion. An effective antitumor effect was, however, still observed. Mechanism of the cytotoxic action of the ADC is considered to be both a result of direct and bystander effects.[25] The active form of MMAE (free MMAE) could be released from the anti-human ADC in peripheral cancer cells, and this small molecule could penetrate into the center of tumor. The anti-human ADC, therefore, had an effective antitumor effect.

Meanwhile, the anti-mouse ADC and control ADC were located in the cancer stroma. Although the anti-mouse ADC might be captured by the cancer stroma cells or extracellular components of tumor stroma, control ADC was also located in the cancer stroma due to EPR effect. In the human cancer tissue, the hTF was highly expressed in cancer stromal cells, such as fibroblasts, pericytes and endothelial cells of tumor vessels, and inflammatory cells.[17] Unexpectedly, the expressions of mTF in the cancer stroma cells were not very high in the experimental subcutaneous tumor model using human cancer cells. Indeed, the biodistribution, location and antitumor effect using the anti-mouse ADC and control ADC were almost same probably based on EPR effect.

We previously reported that the clone 1849 could inhibit both the cell signal pathway *via* PAR2 and the blood coagulation cascade *via* factor VII.[22] The antitumor effect of the anti-human TF mAb used in this study was not effective compared to that of saline group, thus, this might be a result of the cytotoxic drug MMAE not a result of the direct effect of the mAb clone 1849. Similar result was observed in a phase 3 trial of the trastuzumab emtansine (T-DM1).[26] The patients enrolled in the phase 3 trial were previously treated with a taxane and trastuzumab. One of the causes of resistance to trastuzumab is the active mutation of PIK3CA. In the EMILIA trial, PIK3CA mutations were associated with shorter median progression-free survival in the lapatinib plus capecitabine treatment group; however, PIK3CA mutations did not significantly affect the T-DM1 treatment group. These data indicate that the antibody component of the ADC was used as a drug carrier regardless of its own antitumor effect.

More recently, the ADC conjugated with anti-human TF mAb in several solid tumors was reported.[27] On the other hand, in this study, we investigated the antitumor activity of ADC conjugated with not only anti-human TF mAb but also anti-mouse TF mAb. Recently, we reported a cancer stromal target (CAST) therapy consisted of the anticancer drug and mAb against cancer stroma, such as collagen IV or insoluble fibrin.[28–30] The anti-mouse ADC used in this study was also categorized by the CAST therapy because the anti-mouse ADC appeared to damage the host tumor vessels located in the tumor stroma. We think that the anti-TF ADC may become a dual targeting drug in human use because of the present clear evidence that anti-human ADC could damage cancer cells and anti-mouse ADC could damage tumor vessels in the cancer stroma.

Acknowledgements

The authors thank Ms. Misato Kanzaki for her technical assistance and Ms. Kaoru Shiina for her secretarial assistance.

References

1. Siegel R, Naishadham D, Jemal A. Cancer statistics, 2013. *CA Cancer J Clin* 2013;63:11–30.
2. Matsuda T, Ajiki W, Marugame T, Ioka A, Tsukuma H, Sobue T. Research Group of Population-Based Cancer Registries of J. Population-based survival of cancer patients diagnosed between 1993 and 1999 in japan: a chronological and international comparative study. *Jpn J Clin Oncol* 2011;41:40–51.
3. Burris HA,3, Moore MJ, Andersen J, Green MR, Rothenberg ML, Modiano MR, Cripps MC, Portenoy RK, Storniolo AM, Tarassoff P, Nelson R, Dorr FA, et al. Improvements in survival and clinical benefit with gemcitabine as first-line therapy for patients with advanced pancreas cancer: a randomized trial. *J Clin Oncol* 1997;15:2403–13.
4. Cunningham D, Chau I, Stocken DD, Valle JW, Smith D, Steward W, Harper PG, Dunn J, Tudur-Smith C, West J, Falk S, Crellin A, et al. Phase III randomized comparison of gemcitabine versus gemcitabine plus capecitabine in patients with advanced pancreatic cancer. *J Clin Oncol* 2009;27:5513–8.
5. Colucci G, Labianca R, Costanzo D, Gebbia F, Carteni V, Massidda G, Dapretto B, Manzione E, Piazza L, Sannicolo E, Ciaparrone M, Cavanna ML, et al. Randomized phase III trial of gemcita-

bine plus cisplatin compared with single-agent gemcitabine as first-line treatment of patients with advanced pancreatic cancer: the GIP-1 study. *J Clin Oncol* 2010;28:1645–51.
6. Philip PA, Benedetti J, Corless CL, Wong R, O'Reilly EM, Flynn PJ, Rowland KM, Atkins JN, Mirtsching BC, Rivkin SE, Khorana AA, Goldman B, et al. Phase III study comparing gemcitabine plus cetuximab versus gemcitabine in patients with advanced pancreatic adenocarcinoma: southwest oncology Group-directed intergroup trial S0205. *J Clin Oncol* 2010;28:3605–10.
7. Trousseau A. Phlegmasia alba dolens. *Clinique Medicale De l'Hotel-Dieu De Paris* 1865;3:654–712.
8. Billroth T. Lectures on surgical pathology and therapeutics: a handbook for students and practitioners, 8th ed., vol. 2. London: The New Sydenham Society, 1878.
9. Matsumura Y, Kimura M, Yamamoto T, Maeda H. Involvement of the kinin-generating cascade in enhanced vascular permeability in tumor tissue. *Jpn J Cancer Res* 1988;79:1327–34.
10. Dvorak HF. Vascular permeability factor/vascular endothelial growth factor: a critical cytokine in tumor angiogenesis and a potential target for diagnosis and therapy. *J Clin Oncol* 2002;20:4368–80.
11. Stein PD, Beemath A, Meyers FA, Skaf E, Sanchez J, Olson RE. Incidence of venous thromboembolism in patients hospitalized with cancer. *Am J Med* 2006;119:60–8.
12. Ruf W. Molecular regulation of blood clotting in tumor biology. *Haemostasis* 2001;31Suppl1:5–7.
13. Bazan JF. Structural design and molecular evolution of a cytokine receptor superfamily. *Proc Natl Acad Sci USA* 1990;87:6934–8.
14. van den Berg YW, Osanto S, Reitsma PH, Versteeg HH. The relationship between tissue factor and cancer progression: insights from bench and bedside. *Blood* 2012;119:924–32.
15. Drake TA, Morrissey JH, Edgington TS. Selective cellular expression of tissue factor in human tissues. Implications for disorders of hemostasis and thrombosis. *Am J Pathol* 1989;134:1087–97.
16. Flossel C, Luther T, Muller M, Albrecht S, Kasper M. Immunohistochemical detection of tissue factor (TF) on paraffin sections of routinely fixed human tissue. *Histochemistry* 1994;101:449–53.
17. Lorenzet R, Napoleone E, Celi A, Pellegrini G, Di Santo A. Cell-cell interaction and tissue factor expression. *Blood Coagul Fibrinolysis* 1998;9Suppl1:S49–59.
18. Teicher BA, Chari RV. Antibody conjugate therapeutics: challenges and potential. *Clin Cancer Res* 2011;17:6389–97.
19. Thudium K, Bilic S, Leipold D, Mallet W, Kaur S, Meibohm B, Erickson H, Tibbitts J, Zhao H, Gupta M. American Association of Pharmaceutical Scientists National Biotechnology Conference Short Course: Translational Challenges in Developing Antibody–Drug Conjugates: May 24, 2012, San Diego, CA. *MAbs* 2013;5:5–12.
20. Flygare JA, Pillow TH, Aristoff P. Antibody-drug conjugates for the treatment of cancer. *Chem Biol Drug Des* 2013;81:113–21.
21. Matsumura Y, Maeda H. A new concept for macromolecular therapeutics in cancer chemotherapy: mechanism of tumoritropic accumulation of proteins and the antitumor agent smancs. *Cancer Res* 1986;46:6387–92.
22. Saito Y, Hashimoto Y, Kuroda J, Yasunaga M, Koga Y, Takahashi A, Matsumura Y. The inhibition of pancreatic cancer invasion-metastasis cascade in both cellular signal and blood coagulation cascade of tissue factor by its neutralisation antibody. *Eur J Cancer* 2011;47:2230–9.
23. Ducry L, Stump B. Antibody–drug conjugates: linking cytotoxic payloads to monoclonal antibodies. *Bioconjug Chem* 2010;21:5–13.
24. Katz J, Janik JE, Younes A. Brentuximab vedotin (SGN-35). *Clin Cancer Res* 2011;17:6428–36.
25. Okeley NM, Miyamoto JB, Zhang X, Sanderson RJ, Benjamin DR, Sievers EL, Senter PD, Alley SC. Intracellular activation of SGN-35, a potent anti-CD30 antibody–drug conjugate. *Clin Cancer Res* 2010;16:888–97.
26. Verma S, Miles D, Gianni L, Krop IE, Welslau M, Baselga J, Pegram M, Oh DY, Dieras V, Guardino E, Fang L, Lu MW, et al. Trastuzumab emtansine for HER2-positive advanced breast cancer. *N Engl J Med* 2012;367:1783–91.
27. Breij EC, de Goeij BE, Verploegen S, Schuurhuis DH, Amirkhosravi A, Francis J, Miller VB, Houtkamp M, Bleeker WK, Satijn D, Parren PW. An Antibody–drug conjugate that targets tissue factor exhibits potent therapeutic activity against a broad range of solid tumors. *Cancer Res* 2014;74:1214–26.
28. Yasunaga M, Manabe S, Tarin D, Matsumura Y. Cancer-stroma targeting therapy by cytotoxic immunoconjugate bound to the collagen 4 network in the tumor tissue. *Bioconjug Chem* 2011;22:1776–83.
29. Yasunaga M, Manabe S, Tarin D, Matsumura Y. Tailored immunoconjugate therapy depending on a quantity of tumor stroma. *Cancer Sci* 2013;104:231–7.
30. Matsumura Y. Cancer stromal targeting (CAST) therapy. *Adv Drug Deliv Rev* 2012;64:710–9.

Biomaterials 39 (2015) 23–30

Contents lists available at ScienceDirect

Biomaterials

journal homepage: www.elsevier.com/locate/biomaterials

Antibody fragment-conjugated polymeric micelles incorporating platinum drugs for targeted therapy of pancreatic cancer

Jooyeon Ahn [a], Yutaka Miura [b], Naoki Yamada [d], Tsukasa Chida [a], Xueying Liu [b], Ahram Kim [a], Ryuta Sato [e], Ryo Tsumura [e], Yoshikatsu Koga [e], Masahiro Yasunaga [e], Nobuhiro Nishiyama [d], Yasuhiro Matsumura [e], Horacio Cabral [a], Kazunori Kataoka [a, b, c, *]

[a] Department of Bioengineering, Graduate School of Engineering, The University of Tokyo, 7-3-1 Hongo, Bunkyo-ku, Tokyo 113-8656, Japan
[b] Division of Clinical Biotechnology, Center for Disease Biology and Integrative Medicine, Graduate School of Medicine, The University of Tokyo, 7-3-1 Hongo, Bunkyo-ku, Tokyo 113-0033, Japan
[c] Department of Materials Engineering, Graduate School of Engineering, The University of Tokyo, 7-3-1 Hongo, Bunkyo-ku, Tokyo 113-8656, Japan
[d] Polymer Chemistry Division, Chemical Resources Laboratory, Tokyo Institute of Technology, R1-11, 4259 Nagatsuta, Midori-ku, Yokohama 226-8503, Japan
[e] Division of Developmental Therapeutics, National Cancer Center Hospital East, 6-5-1 Kashiwanoha, Kashiwa, Chiba 277-8577, Japan

ARTICLE INFO

Article history:
Received 13 August 2014
Accepted 20 October 2014
Available online 15 November 2014

Keywords:
Drug delivery
Platinum
Micelle
Nanoparticle
Chemotherapy

ABSTRACT

Antibody-mediated therapies including antibody-drug conjugates (ADCs) have shown much potential in cancer treatment by tumor-targeted delivery of cytotoxic drugs. However, there is a limitation of payloads that can be delivered by ADCs. Integration of antibodies to drug-loaded nanocarriers broadens the applicability of antibodies to a wide range of therapeutics. Herein, we developed antibody fragment-installed polymeric micelles *via* maleimide-thiol conjugation for selectively delivering platinum drugs to pancreatic tumors. By tailoring the surface density of maleimide on the micelles, one tissue factor (TF)-targeting Fab' was conjugated to each carrier. Fab'-installed platinum-loaded micelles exhibited more than 15-fold increased cellular binding within 1 h and rapid cellular internalization compared to non-targeted micelles, leading to superior *in vitro* cytotoxicity. *In vivo*, Fab'-installed micelles significantly suppressed the growth of pancreatic tumor xenografts for more than 40 days, outperforming non-targeted micelles and free drugs. These results indicate the potential of Fab'-installed polymeric micelles for efficient drug delivery to solid tumors.

1. Introduction

Antibody-drug conjugates (ADCs) are attracting much interest in cancer therapy [1,2] due to the improvement of therapeutic efficacies by selectively delivering anticancer drugs to cancer cells compared to conventional chemotherapies. The development of ADCs has been one of the most active areas in recent years, and as much as thirty ADCs have entered clinical evaluation in 2013 for the treatment of solid tumors and leukemia [3]. Nevertheless, a major challenge in the development of ADCs is the limited amounts of drugs that can be delivered by a single antibody, as overloading may reduce the binding affinity of the antibody or affect the pharmacokinetics [4,5]. Thus, 2 to 4 cytotoxins per antibody are generally introduced in an ADC for accomplishing effective therapeutic responses without compromising the affinity of the antibody [6,7]. Consequently, the drugs conjugated to the antibody must be highly cytotoxic, such as auristatins [8,9], maytansines [10,11] and calicheamicins [12], which are 100–1000 times higher than typical anticancer drugs, for exerting enough efficacy, although there are growing concerns over side effects from decomposition of ADC under physiological conditions [13,14]. However, these obstacles of ADCs may be overcome by integrating antibodies to drug-loaded nanocarriers, which are capable of delivering a significantly higher amount than ADCs [15].

Among long-circulating nanocarriers with improved tumor extravasation and penetration, polymeric micelles offer substantial benefits as platform nanocarriers for conjugating antibodies. Polymeric micelles present high and versatile loading of bioactive molecules and their controlled release, and show prolonged blood circulation (stealth property) due to their surface coverage by biocompatible PEG strands [16–19]. Besides the relative small size of micelles ranging from 10 to 100 nm, they exhibit enhanced

* Corresponding author. Department of Materials Engineering, Graduate School of Engineering, The University of Tokyo, 7-3-1 Hongo, Bunkyo-ku, Tokyo 113-8656, Japan. Tel.: +81 3 5841 7138; fax: +81 3 5841 7139.
E-mail address: kataoka@bmw.t.u-tokyo.ac.jp (K. Kataoka).

http://dx.doi.org/10.1016/j.biomaterials.2014.10.069
0142-9612/

tumor accumulation by the enhanced permeability and retention (EPR) effect through leaky vasculatures and impaired lymphatic drainage in solid tumors [20,21]. To date, a few antibody-conjugated micelles (immunomicelles) were reported for specific delivery of drugs in cancer therapy. One of the earliest immunomicelles were paclitaxel-loaded lipid-micelles conjugating nucleosome-targeting 2C5 antibody on their surface for specific targeting of breast adenocarcinoma and Lewis lung carcinoma [22,23]. Recently, epidermal growth factor receptor (EGFR)-targeting [24] and HER-2-targeting immunomicelles incorporating doxorubicin [25], and hypoxia inducible factor 1 (HIF-1)-targeting paclitaxel-loaded immunomicelles [26] have shown enhanced efficacy toward antigen-overexpressing cancer cells, indicating the high potential of immunomicelles in targeted cancer therapy. However, no immunomicelle has proceeded to clinical evaluation so far. Therefore, using micellar platform with high potential for clinical translation should facilitate the development of anticancer therapies based on immunomicelle.

Herein, we introduced the antibody fragments to polymeric micelles incorporating an active complex of oxaliplatin, (1,2-diaminocyclohexane)platinum(II) (DACHPt) (DACHPt/m), which have shown strong therapeutic activity against several cancer models and are being evaluated in phase I clinical studies [27]. DACHPt/m are self-assembled by the polymer-metal complex formation between the carboxylates of poly(glutamic acid) of poly(-ethylene glycol)-*b*-poly(glutamic acid) (PEG-*b*-P(Glu)) copolymers and the platinum drug [28]. The release of the incorporated DACHPt from the micelles is triggered by the ligand exchange of Pt(II) from the carboxylates in the block copolymer to chloride ions in the media, and is further accelerated at low pH conditions [29]. Accordingly, DACHPt/m stably circulate in the bloodstream in micelle form with minimal drug release, and after accumulating in tumor tissues and being endocytosed by cancer cells, the drug release from DACHPt/m is accelerated due the low pH and high chloride ion concentration of late endosomes/lysosomes. By conjugating antibody fragments to DACHPt/m, DACHPt/m could improve the efficacy of the loaded platinum drugs by enhanced delivery to tumor cells and effective intracellular drug release. In this regards, we may maximize therapeutic effects through antibody-antigen recognition and cellular uptake. As an antibody, we selected our recently developed anti-tissue factor (TF) antibody (clone 1849), which can target TF overexpressed on the surface of cancer cells, such as human pancreatic, colorectal, breast and lung cancers [30–32], as well as tumor associated monocytes and endothelial cells [31,33]. In fact, this anti-TF antibody demonstrated efficient targeting abilities including inhibition of the invasion and metastasis [34]. Accordingly, the development of these anti-human TF-antibody Fab' fragment-conjugated DACHPt/m (anti-TF Fab'-DACHPt/m) was studied in detail to determine their potential as a versatile target antigen for tumor-selective drug delivery. These immunomicelles were further evaluated against a tumor model of pancreatic cancer, because it is one of the most challenging models for drug delivery [35,36] and the application of antibody-antigen systems to polymeric micelles may positively impact on its clinical treatment. Our results highlight the potential of this approach for constructing Fab'-installed polymeric micelles for efficient drug delivery to tumors.

2. Materials and methods

2.1. Materials

α-Methoxy-ω-amino poly(ethylene glycol) (MeO-PEG-NH_2; M_n: 12,000), *N*-carboxyl anhydride of γ-Benzyl-L-glutamate (NCA-BLG) were purchased from NOF Co., Inc. (Tokyo, Japan) and Chuo Kaseihin Co., Inc. (Tokyo, Japan), respectively. Dimethyl formamide (DMF), dimethyl sulfoxide (DMSO), dithiothreitol (DTT), *N*-(4-Maleimidobutyryloxy)-sulfosuccinimide, sodium salt (Sulfo-GMBS), sodium sulfate decahydrate ($Na_2SO_4 \cdot 10H_2O$), oxaliplatin and phosphate buffered saline (PBS) were obtained from Wako Pure Chemical Co., Inc. (Osaka, Japan). MeO-PEG-*b*-P(Glu) was synthesized as previously described synthetic method [28]. MeO-PEG-*b*-P(Glu); yield = 97%, the degree of polymerization of the P(Glu) ($DP_{P(Glu)}$) = 40, $M_{n,NMR}$ = 18,000. ^{1}H NMR (400 MHz, D_2O): δ (ppm) = 1.70–2.55 (−C<u>H</u>$_2$−C<u>H</u>$_2$−P(Glu) side chain), 3.30 (−O−C<u>H</u>$_3$), 3.45–3.85 (−C<u>H</u>$_2$−C<u>H</u>$_2$−O−PEG backbone), 4.20–4.40 (−C<u>H</u>−P(Glu) backbone). Mal-PEG-*b*-P(Glu) was synthesized based on our previously reported method [37]. Mal-PEG-*b*-P(Glu); yield = 94%, $DP_{P(Glu)}$ = 40, ^{1}H NMR (400 MHz, D_2O): δ (ppm) = 1.70–2.65 (−C<u>H</u>$_2$−C<u>H</u>$_2$−P(Glu) side chain), 3.35 (−$(CH_2)_3$−CO−NH−C<u>H</u>$_2$−), 3.50–3.92 (−C<u>H</u>$_2$−C<u>H</u>$_2$−O−PEG backbone), 4.12–4.46 (−C<u>H</u>−P(Glu) backbone), 6.85 (−C<u>H</u>=C<u>H</u>− maleimide group). Dichloro(1,2-diaminocyclohexane)platinum(II) (DACHPtCl_2) was purchased from Heraeus (Hanau, Germany). $AgNO_3$ was purchased from Aldrich Chemical Co., Inc. (Milwaukee, WI). BCA protein assay reagent was purchased from Pierce Chemical Co., Inc. (Rockford, IL). Alexa Fluor 647-succinimidyl esters, Alexa Fluor 488-TFP ester, Hoechst 33342, and LysoTracker Green were purchased from Invitrogen Molecular Probes (Eugene, OR). Rhodamine 6G was purchased from Sigma–Aldrich Co., Inc. (St. Louis, MO). Anti-human tissue factor antibody (1849c, F(ab')$_2$) and anti-mouse tissue factor antibody (1157c, F(ab')$_2$) were purchased from ITM Co., Ltd. (Nagano, Japan). Fetal bovine serum (FBS) was purchased from Dainippon Sumitomo Pharma Co., Ltd. (Osaka, Japan). Cell Counting Kit-8 was obtained from Dojindo Laboratories (Kumamoto, Japan).

2.2. Cell lines and animals

Human pancreatic cancer BxPC3 cells were obtained from American Type Culture Collection (Manassas, VA). The BxPC3 cells were maintained in RPMI 1640 medium (Sigma Chemical Co., Inc., St. Louis, MO) supplemented with 10% (v/v) FBS, 1% penicillin/streptomycin in a humidified atmosphere containing 5% CO_2 at 37 °C. BALB/c nu/nu mice (18–20 g body weight; female; age, 6 weeks) were purchased from Charles River Japan (Kanagawa, Japan). All animal experiments were performed in accordance with the Guidelines for the Care and Use of Laboratory Animals as stated by the University of Tokyo.

2.3. Preparation of antibody fragment Fab' with thiols

To obtain Fab' fragment having thiol residues, F(ab')$_2$ fragments of anti-human TF antibody (0.5 mg/mL) were stirred with different concentrations of DTT from 0.5 μM to 5 mM for 30 min at 37 °C. The crude product was purified by ultrafiltration 4 times (MWCO: 30,000). The purity of Fab' fragment was confirmed by aqueous phase GPC (JASCO HPLC system, Easton, MD), which equipped with UV detector and a Superdex™ 200 10/300 GL column (GE healthcare, Ltd., Buckinghamshire, UK), with eluent of 10 mM phosphate buffer (pH 7.4) containing 150 mM NaCl at a flow rate of 0.75 mL/min at room temperature. For the fluorescence-labeling, anti-human TF F(ab')$_2$ (1 mg/mL) was combined with Alexa Fluor 488 in 1M $NaHCO_3$ solution at room temperature. After 1 h stirring, the Alexa 488-labeled F(ab')$_2$ was separated from non-conjugated free Alexa dye by PD-10 column. The labeled F(ab')$_2$ was then treated by DTT in the same manner as explained in above to afford Alexa 488-labeled anti-TF Fab' fragment having thiol residues.

2.4. Preparation and characterization of maleimide-functionalized DACHPt-loaded micelles (Mal-DACHPt/m)

MeO-PEG-*b*-P(Glu) and Mal-PEG-*b*-P(Glu) (total [Glu] = 5 mM) were mixed with DACHPt$(NO_3)Cl$ (5 mM) in distilled water at 37 °C, for preparation of 50% Mal-DACHPt/m [MeO-PEG-*b*-P(Glu)]/[Mal-PEG-*b*-P(Glu)] = 1.0/1.0 (mol/mol)] and 20% Mal-DACHPt/m [4.0/1.0 (mol/mol)]. The obtained micelles were purified by dialysis (Spectra/Pro 6 Membrane: MWCO: 6-8,000), followed by ultrafiltration (MWCO: 30,000) to afford Mal-DACHPt/m. The size and distribution of both Mal-DACHPt/m were estimated by dynamic light scattering (DLS: Malvern Instruments Ltd., UK, at 532 nm, 25 °C) measurement. The content of Pt in the micelles was measured by the inductively coupled plasma mass spectrometry (ICP-MS: Agilent 7700 series ICP-MS, Agilent Technologies, Inc., Santa Clara, CA). The association degree of Pt and carboxylic acid in P(Glu) was calculated by the Pt contents and freeze-dried weight of the micelles. Alexa 647-labeled Mal-DACHPt/m were obtained by using Alexa Fluor 647-labeled MeO-PEG-*b*-P(Glu) [37].

2.5. Preparation and characterization of antibody fragment-conjugated micelles

Anti-TF Fab' was conjugated to 50% Mal-DACHPt/m or 20% Mal-DACHPt/m by incubation at room temperature overnight to afford immunomicelles. Before the conjugation reaction, the concentration of antibody was determined by BCA protein assay kit with anti-TF Fab' antibody as the standard. The feed ratio between maleimide groups of Mal-DACHPt/m and anti-TF Fab' was 17.0/1.0 (mol/mol) for preparation of 50% Mal-DACHPt/m and 6.8/1.0 (mol/mol) for that of 20% Mal-DACHPt/m. The conjugation of antibody fragments to Mal-DACHPt/m was confirmed with fluorescence correlation spectroscopy using a Zeiss LSM 510 META equipped with FCS setup ConfoCor 3 (Carl Zeiss, Germany). The fluorescence of Alexa 488-labeled Fab' fragments was detected with a 488 nm Argon laser for excitation and a 530 nm band-pass filter for emission before and after the conjugation with non-fluorescence labeled 20% Mal-DACHPt/m or 50% Mal-DACHPt/m. After the

measurement, the diffusion time of Fab' fragments and immunomicelles were calculated from the autocorrelation curves. Diffusion coefficient was then calculated based on the diffusion times of micelles and Rhodamine 6G as standard fluorescence molecule.

2.6. In vitro evaluation of anti-TF Fab'-DACHPt/m by flow cytometry

Alexa 647 fluorescence-labeled anti-TF Fab'-DACHPt/m or DACHPt/m were added to BxPC3 cells (1×10^5 cells in 100 μL medium) and incubated at 4 °C for 1 h, without light exposure. Cells were washed four times with fresh medium to remove unbound micelles, resuspended in PBS and the mean fluorescence intensities were measured by flow cytometry (Becton Dickinson LSR II) and analyzed by BD FACSDiVa software. During the measurement, 10,000 events were counted per each sample. For the competition assay, the 10-fold excess of free anti-human TF $F(ab')_2$ fragments were co-incubated with Alexa 647-labeled anti-TF Fab'-DACHPt/m with BxPC3 cells, and the experiment was carried out as described above.

2.7. Assessment of cellular uptake by confocal laser scanning microscopy (CLSM)

The fluorescence intensity of micelles was adjusted to equal intensity by Nanodrop 3300 (RFU = 8,000). Alexa 647-labeled DACHPt/m or anti-TF Fab'-DACHPt/m were added to BxPC3 cells (1.6×10^4 cells in 200 μL medium) in Lab-Tek 8-well chambered coverglass (Thermo, Rochester, NY). After determined time periods, the cells were washed twice with fresh medium, stained with Hoechst 33342, and imaged with CLSM using a Zeiss LSM 780 (Carl Zeiss, Germany). The fluorescence was quantified by measuring the mean pixel intensities from Alexa 647-labeled micelles in cell areas using the LSM software ($n = 25$). The statistical significance of cellular uptake was determined by Student's *t*-test. By staining with LysoTracker Green, the colocalization of Alexa 647-labeled-anti-TF Fab'-DACHPt/m with late endosomal/lysosomal compartments was assessed.

2.8. In vitro cytotoxicity

The 50 percent inhibitory concentration (IC_{50}) of free oxaliplatin, DACHPt/m, anti-TF Fab'-DACHPt/m and anti-TF Fab' was evaluated by cytotoxicity assay against BxPC3 cells. The cells were exposed to the drugs for 3 h, followed by washing three times with fresh medium and post-incubated for 48 h. Then, the viability of cells was measured by using Cell Counting Kit-8. For the cytotoxicity evaluation of anti-TF Fab', the cells were continuously exposed to the antibody fragments for 48 h, and the viability of the cells was investigated as aforementioned.

2.9. In vivo antitumor activity assay on BxPC3 subcutaneous tumor model

To prepare BxPC3 subcutaneous xenografts, BALB/c nu/nu mice (6 week old, female) were inoculated with 5×10^6 cells. When the average tumor volume reached 50 mm^3, mice were i.v. injected from the tail vein at 3 times every fourth day with saline (PBS), oxaliplatin (8 mg/kg), DACHPt/m (3 mg/kg), anti-TF Fab'-DACHPt/m (3 mg/kg), and co-injection of Mal-DACHPt/m (3 mg/kg) and anti-TF Fab'. The tumor volume was measured by a caliper and calculated with the use of the following equation:

$$\text{Volume}_{\text{tumor}} = 0.5\ (\text{Major diameter}) \times (\text{Minor diameter})^2$$

The statistical significance of the antitumor activity was determined by Two-way ANOVA test.

2.10. Platinum accumulation on BxPC3 subcutaneous tumor in mouse xenograft

BxPC3 cells (5×10^6 cells in medium) were inoculated to BALB/c nu/nu mice (6 week old, $n = 5$, female) to establish subcutaneous BxPC3 tumor model. When the average tumor size is reached c.a. 100 mm^3, anti-TF Fab'-DACHPt/m, DACHPt/m and oxaliplatin were intravenously injected into the tail vein at 5 mg/kg on a DACHPt basis. Mice were sacrificed after 1, 6 and 24 h injection. Tumors were excised and decomposed with nitric acid on a hot plate until the samples became dried. Approximately 1.0 mL of nitric acid (1 vol%, 1.0 mL) was added to the samples to be dissolved, then the platinum concentration in the solution was measured by ICP-MS.

3. Results and discussion

3.1. Preparation of maleimide-functionalized DACHPt-loaded micelles

The block copolymers such as methoxy-poly(ethylene glycol)-*b*-poly(glutamic acid) (MeO-PEG-*b*-P(Glu), polymer 1 in Fig. 1) copolymer and maleimide-PEG-*b*-P(Glu) copolymer (Mal-PEG-*b*-P(Glu), polymer 2 in Fig. 1) were added to DACHPt aqueous solution to prepare the maleimide-functionalized DACHPt-loaded micelles (Mal-DACHPt/m) [37,38]. During this process, the coordinate covalent bonds occurred between the platinum atom and the carboxylate groups of poly(glutamic acid), and then triggered their self-assembling to form core-shell micelles, with DACHPt in their core and maleimide moieties on their PEG shell (Fig. 1) [28,39]. The proportion of maleimide functionality on the shell of micelles was controlled for optimizing the conjugation of antibody fragments by directly adjusting the ratio of polymer 1 and polymer 2. In this way, we prepared Mal-DACHPt/m with different maleimide density in the surface of micelle such as 20% Mal-DACHPt/m and 50% Mal-DACHPt/m. The diameter of these Mal-DACHPt/m was approximately 30 nm with narrow distribution, as determined by dynamic light scattering measurements (DLS), which was comparable to that of DACHPt/m prepared from MeO-PEG-*b*-P(Glu) (Table 1). The complexation ratio of Pt to carboxylate ([Pt]/[COO] = mol/mol) and the drug loading of Mal-DACHPt/m (Pt/polymer = wt/wt%) were also comparable to that of DACHPt/m (Table 1). The maleimide

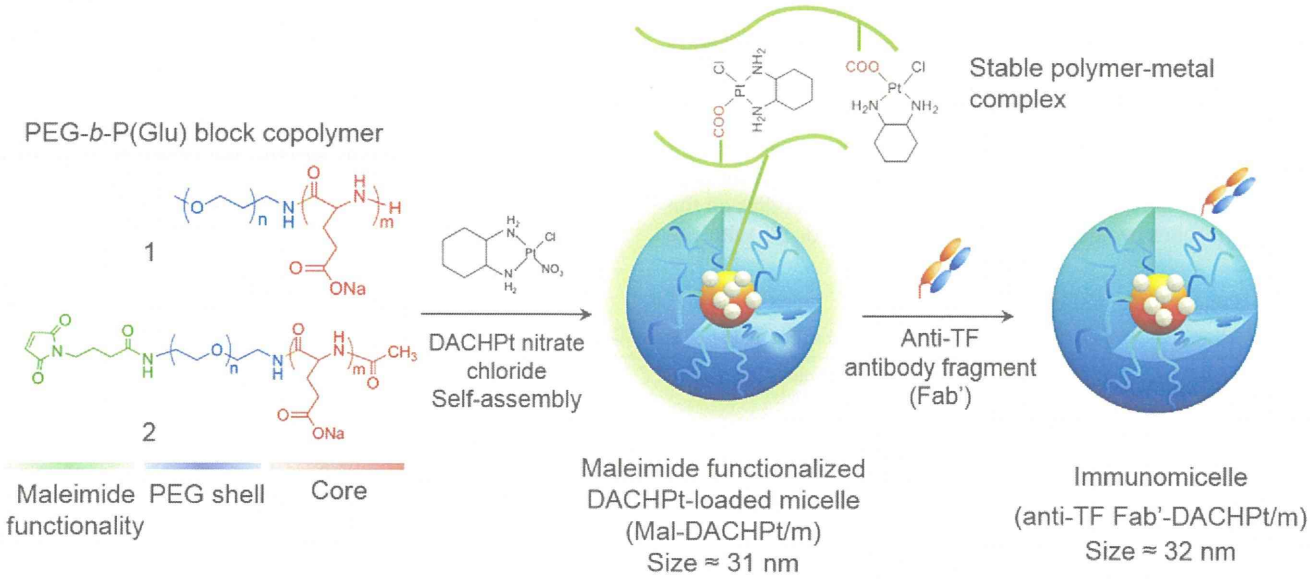

Fig. 1. Schematic illustration of the preparation of anti-TF Fab' fragment-installed DACHPt/m.

Table 1
Characterization of maleimide-functionalized DACHPt/m.

Micelles	Size [nm][a]	PDI[b]	[Pt]/[COO][c] [mol/mol]	Pt/polymer[c] [wt/wt%]
DACHPt/m	30	0.09	0.48	46
20% Mal-DACHPt/m	28	0.09	0.46	44
50% Mal-DACHPt/m	31	0.10	0.47	45
anti-TF Fab'-DACHPt/m[d]	32	0.17	0.45	44

[a] Volume averaged diameter determined by DLS.
[b] Polydispersity index determined by DLS.
[c] Determined by ICP-MS.
[d] Anti-TF Fab'-conjugated 50% Mal-DACHPt/m.

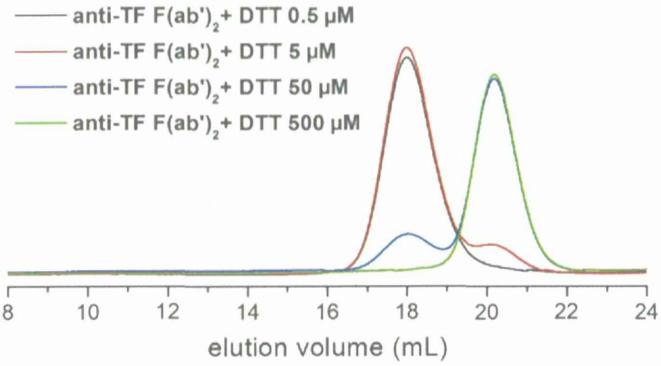

Fig. 2. GPC chromatograms detected by UV absorption at 220 nm of anti-TF F(ab')$_2$ fragment after DTT treatment with different concentrations.

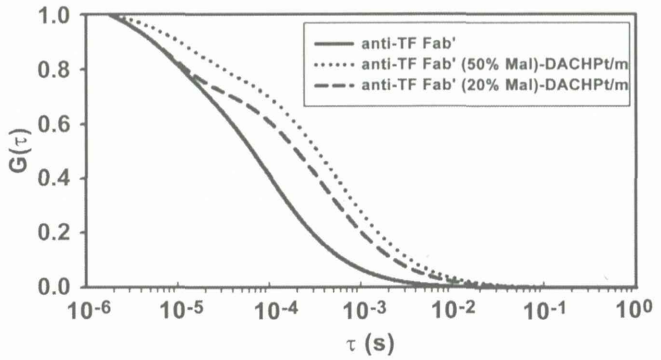

Fig. 3. FCS autocorrelation curves of Alexa 488-labeled anti-TF Fab' fragment before and after the conjugation with 20% Mal-DACHPt/m or 50% Mal-DACHPt/m.

groups on Mal-DACHPt/m allow introducing antibodies through thiol-maleimide reaction, which is a widely used linkage for preparing ADC [40,41]. Moreover, the conjugation of antibodies on the surface of micelles avoids the binding of platinum drugs with the

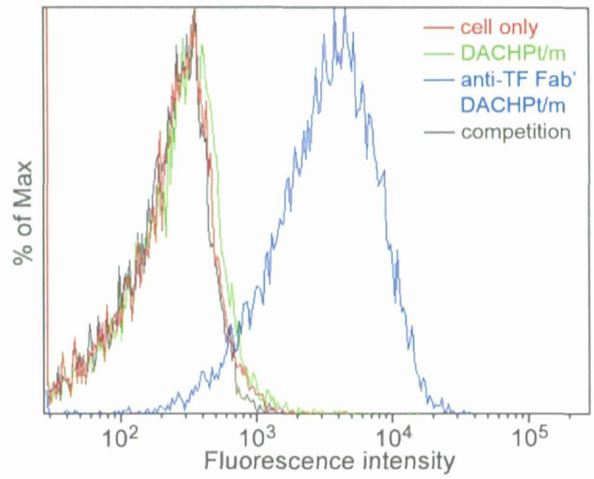

Fig. 4. Binding of Alexa 647-labeled DACHPt/m (green line) and anti-TF Fab'-DACHPt/m (blue line) against human pancreatic cancer BxPC3 cell after 1 h incubation at 4 °C analyzed by flow cytometry. Competition experiments on BxPC3 cells (black line) were performed by co-incubating anti-TF Fab'-DACHPt/m with 10-fold excess free anti-human TF F(ab')$_2$. The cells without any micelles were used as a negative control (red line).

antibodies, which may reduce their binding affinity, and eliminates the potential disturbance of the antibodies on the self-assembly process of the micelles. In addition, because the release of DACHPt from the core of micelles is induced by acidic pH and Cl^-, the conjugation of the antibodies by thiol-maleimide chemistry is a substantial advantage, as it can be performed in water without changing pH, preventing drug leakage [42,43]. Thus, these Mal-DACHPt/m could facilitate the efficient conjugation of antibodies without affecting their properties.

3.2. Conjugation of antibody fragments to maleimide-functionalized DACHPt/m

Thiol-bearing Fab' fragments of anti-human TF antibody (anti-TF Fab') were fabricated by cleaving the interchain disulfide bonds of F(ab')$_2$ through reduction with dithiothreitol (DTT), as these bonds are readily reducible sites, and their cleavage is frequently used for antibody conjugation without losing the binding properties of antibodies [40,43,44]. The optimal reduction conditions for preparing anti-TF Fab' were determined by gel permeation chromatography (GPC) (Fig. 2), following the shift of the peak related to F(ab')$_2$ at 18.0 min to that of anti-TF Fab' at 20.5 min. When 500 μM of DTT was added to the reaction system, we observed only the peak corresponding anti-TF Fab', while F(ab')$_2$ treated with 5 and 50 μM DTT showed the coexistence of F(ab')$_2$ and anti-TF Fab' (Fig. 2). It is worth noticing that, at DTT concentrations higher than 500 μM, Fab'

Table 2
FCS parameters of fluorescently labeled anti-TF Fab' before and after conjugation with Mal-DACHPt/m.

	Correlation[a]	Counts per molecule [kHz][a]	Diffusion time [μs][a]	Diffusion coefficient [μm^2/sec][a]	Hydrodynamic diameter [nm][b]
Anti-TF Fab'	1.03	3.61	92.4 ± 1.6	77.6 ± 1.3	6
Anti-TF Fab' (20% Mal)-DACHPt/m	1.02	2.51	437.1 ± 12.9	16.4 ± 0.5	27
Anti-TF Fab' (50% Mal)-DACHPt/m	1.03	3.66	505.3 ± 6.5	14.2 ± 0.2	31

[a] Correlation, counts per molecule and diffusion time were calculated by ConfoCor 3 software.
[b] Hydrodynamic diameter was calculated by Stokes-Einstein equation.

fragment decomposed into smaller fragments, showing the chromatograms at later elusion times (data not shown). Therefore, we concluded that 500 μM of DTT was the optimal concentration for producing anti-TF Fab'.

The obtained anti-TF Fab' were purified by ultrafiltration, followed by the installation on Mal-DACHPt/m through the formation of thioether bond [6,45]. The conjugation of anti-TF Fab' to Mal-DACHPt/m was studied by following the changes in the diffusion coefficient of Alexa 488-labeled anti-TF Fab' by fluorescence correlation spectroscopy (FCS). From the FCS autocorrelation function curves of Alexa 488-labeled anti-TF Fab' and its conjugated DACHPt/m (anti-TF Fab'-DACHPt/m) (Fig. 3), it was observed that the diffusion coefficient of anti-TF Fab'-DACHPt/m was significantly smaller than that of single anti-TF Fab' (Table 2), indicating the successful conjugation of anti-TF Fab' on Mal-DACHPt/m. In addition, the counts per molecule (CPM), *i.e.* the mean fluorescence intensity per molecule, in single anti-TF Fab' were comparable to that of 50% anti-TF Fab'-DACHPt/m (Table 2), suggesting that one anti-TF Fab' was conjugated to each 50% Mal-DACHPt/m in this reaction setting. The calculated CPM for anti-TF Fab'-DACHPt/m prepared from 20% Mal-DACHPt/m was less than that of single anti-TF Fab'. This implies that the anti-TF Fab'-DACHPt/m obtained from 20% Mal-DACHPt/m were a mixture of micelles with and without Fab'. Therefore, we selected 50% Mal-DACHPt/m for Fab' conjugation. The hydrodynamic diameter of Mal-DACHPt/m remained close to 30 nm even after Fab' conjugation (Tables 1 and 2). This might be reasonable considering the diameter of Fab' as that of a volume-equivalent sphere of 4–6 nm [46] (Table 2). This relatively small size of anti-TF Fab'-DACHPt/m could be a significant advantage for effective extravasation and penetration in stroma-rich tumor tissues of pancreatic cancer [35].

3.3. Binding activity of anti-TF Fab'-DACHPt/m on TF-overexpressing human pancreatic cancer cells

To study the binding of anti-TF Fab'-DACHPt/m to TF-expressing cells, human pancreatic cancer BxPC3 cells, which overexpress TF [47], were exposed to fluorescent-labeled anti-TF Fab'-DACHPt/m

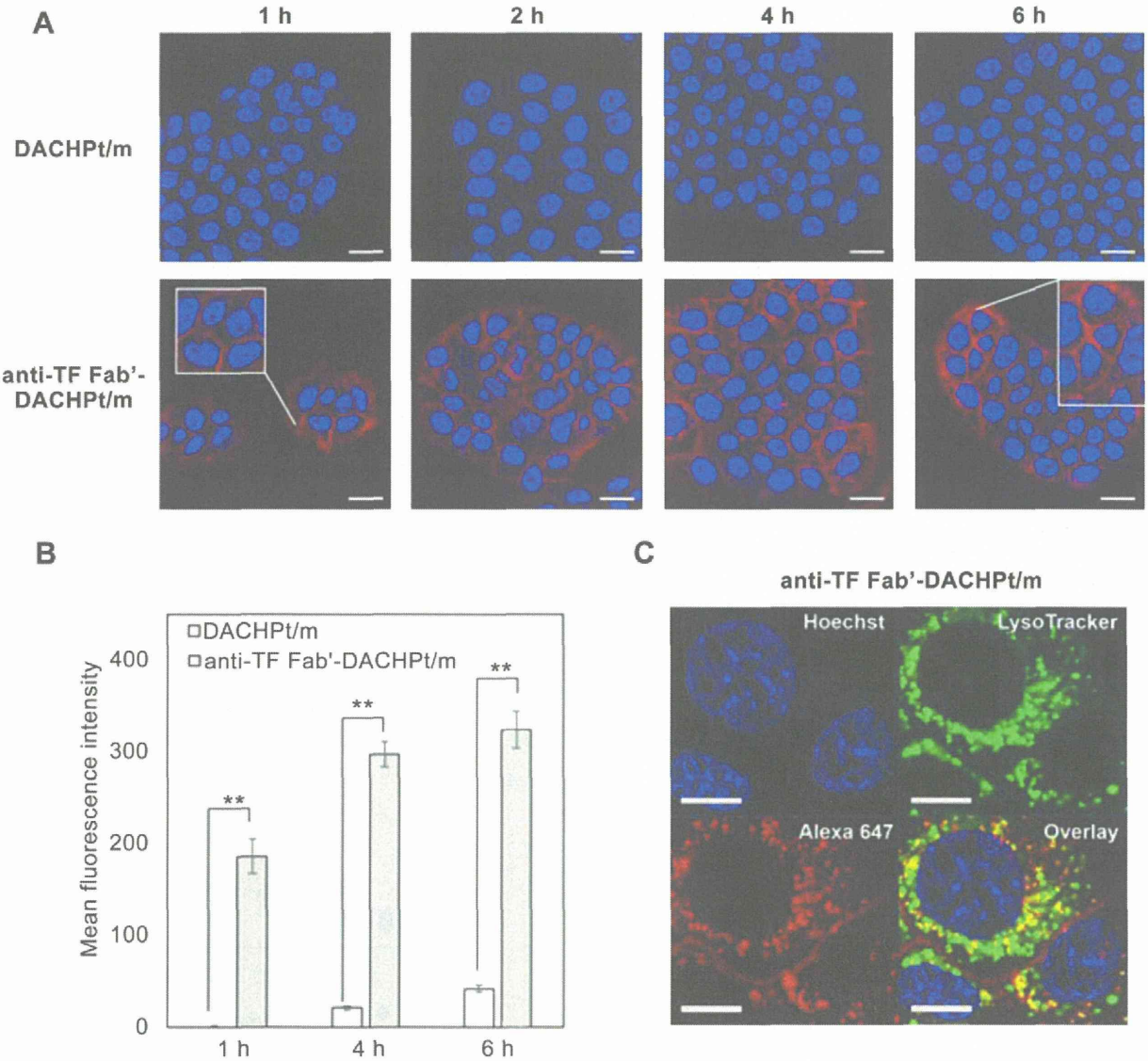

Fig. 5. (A) Representative CLSM images of BxPC3 cells incubated with Alexa 647-labeled DACHPt/m and anti-TF Fab'-DACHPt/m for 1–6 h at 37 °C. The merged images of Hoechst 33342-stained nuclei (blue) and fluorescence-labeled micelles (red) (scale bar = 20 μm); (B) The mean fluorescence intensity of Alexa 647 in BxPC3 cells from images taken at 1, 4, 6 h was quantified ($n = 25$, error bar = ±S.E.M., $^{**}p < 0.001$ calculated by Student's *t*-test); (C) Cellular localization of anti-TF Fab'-DACHPt/m after 6 h exposure against BxPC3 cells at 37 °C. The images show Alexa 647-labeled micelles (red), late endosomes and lysosomes stained by LysoTracker Green (green), nuclei stained by Hoechst 33342 (blue) and their overlay (scale bar = 10 μm).

Table 3
Concentration of drugs for fifty-percent inhibition of the growth of BxPC3 cells.

Cells	IC_{50} [μM][a]			
	Oxaliplatin	DACHPt/m	anti-TF Fab'-DACHPt/m	anti-TF Fab'[b]
BxPC3	23	126	25	N/A

[a] Determined by CCK-8.
[b] Exposed for 48 h.

for 1 h at 4 °C. Then, the amount of micelles bound to the cells was assessed through flow cytometry. The average fluorescence levels in the cells treated with anti-TF Fab'-DACHPt/m (blue line) were more than 15-fold higher than control BxPC3 cells (red line) (Fig. 4), indicating the promoted cellular binding of these micelles after 1 h incubation, while DACHPt/m (green line) did not show any cellular binding. To confirm whether the enhanced cellular association of anti-TF Fab'-DACHPt/m results from the specific binding of anti-TF Fab' to TF on the cell surface, a competition experiment was performed by using 10-fold excess amount of free anti-human TF $F(ab')_2$. The results demonstrated that the cells treated by anti-TF Fab'-DACHPt/m and excess anti-human TF $F(ab')_2$ (Fig. 4; black line) did not show any increase in the fluorescence levels. It is likely that TF on BxPC3 cells were occupied by the excess free $F(ab')_2$, thereby restricting the binding sites for anti-TF Fab'-DACHPt/m. From these results, we concluded that the introduced anti-TF Fab' on DACHPt/m can selectively bind to TF overexpressed on BxPC3 cells. It is worth noting that only one anti-TF Fab' conjugation to each micelle promoted such enhanced binding.

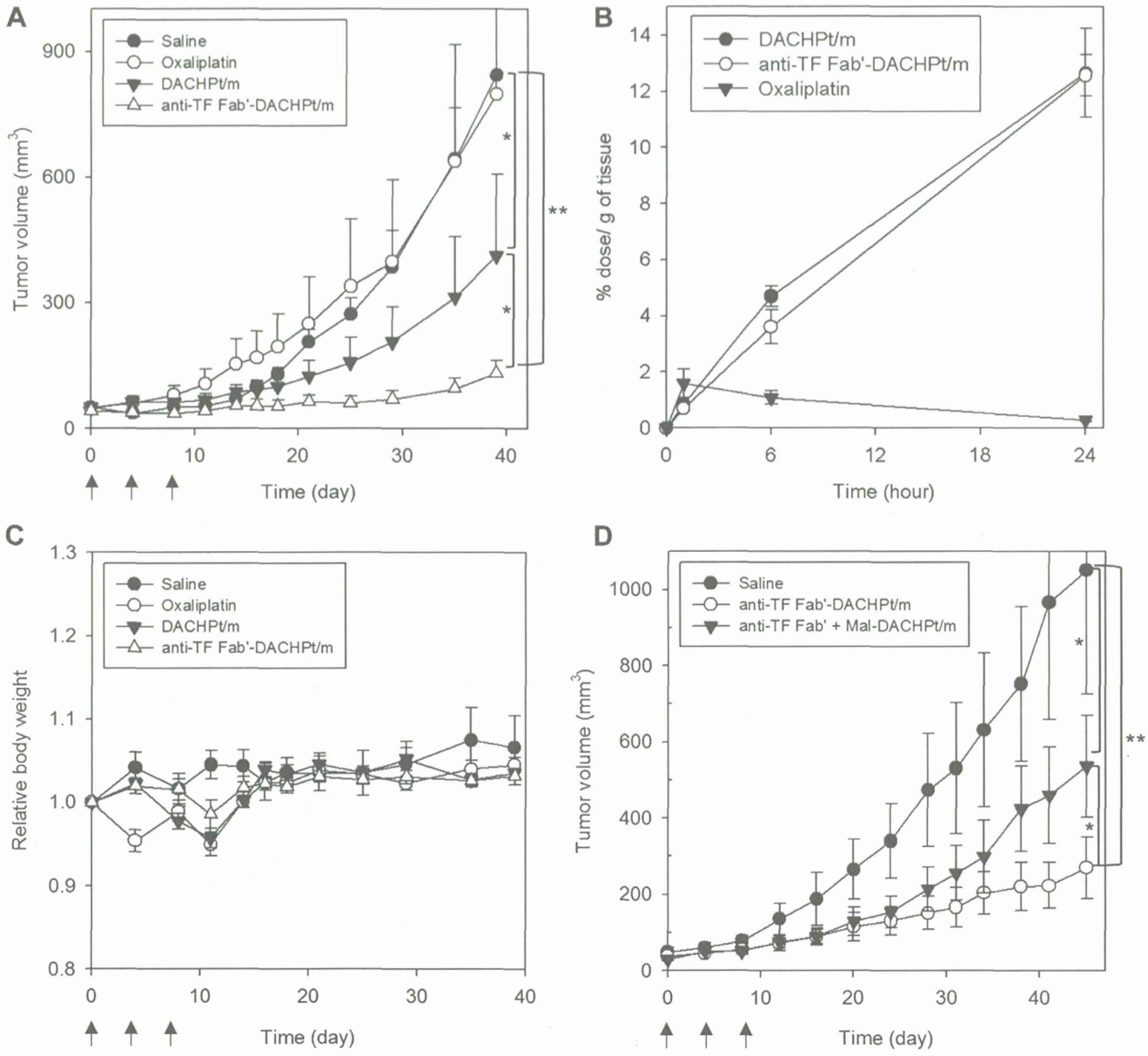

Fig. 6. *In vivo* antitumor efficacy of DACHPt/m series against human pancreatic adenocarcinoma BxPC3 xenografts. (A) The drugs were injected three times as indicated with arrows, every 4th day from day 0 (*$p < 0.01$, **$p < 0.001$ calculated by Two-way ANOVA, Error bars = S.E.M.; $n = 5$). The doses for DACHPt/m and anti-TF Fab'-DACHPt/m were 3 mg/kg on a DACHPt basis, and oxaliplatin for 8 mg/kg; (B) Time profiles of Pt concentration in tumor after i.v. administration into BALB/c nude mice bearing BxPC3 subcutaneous tumor ($n = 5$). The doses for DACHPt/m, anti-TF Fab'-DACHPt/m and oxaliplatin were 5 mg/kg on a DACHPt basis. Error bars = S.E.M.; (C) Relative body weight of the mice during the antitumor activity experiment (A); (D) The doses for co-injection of anti-TF Fab' and Mal-DACHPt/m (anti-TF Fab' + Mal-DACHPt/m) and anti-TF Fab'-DACHPt/m were 3 mg/kg on a DACHPt basis (*$p < 0.01$, **$p < 0.001$ calculated by Two-way ANOVA, Error bars = S.E.M.; $n = 5$).

3.4. Cellular uptake and in vitro cytotoxicity

To confirm cellular internalization of anti-TF Fab' DACHPt/m in BxPC3 cells, we performed confocal laser scanning microscopy (CLSM) evaluation with fluorescence-labeled anti-TF Fab'-DACHPt/m and DACHPt/m (Fig. 5). After 1 h incubation, the fluorescence signal from anti-TF Fab'-DACHPt/m was clearly observed in BxPC3 cells, while DACHPt/m were barely discernable (Fig. 5A). From 2 h to 6 h incubation, the red fluorescence signal (anti-TF Fab'-DACHPt/m) was gradually increased, whereas the fluorescent signal from DACHPt/m was still significantly weak (Fig. 5A). Quantification of fluorescent intensity clearly indicated the rapid binding and internalization of anti-TF Fab'-DACHPt/m against BxPC3 cells (Fig. 5B). By staining the late endosomes and lysosomes with LysoTracker Green (Fig. 5C; green), we confirmed the colocalization (Fig. 5C; yellow) of anti-TF Fab'-DACHPt/m (Fig. 5C; red) and late endosomes/lysosomes in BxPC3 cells, suggesting that anti-TF Fab' promoted cellular uptake. This is in good agreement with previous reports regarding the TF-targeted ADC [47].

The *in vitro* cytotoxicity of anti-TF Fab'-DACHPt/m was studied in BxPC3 cells by exposing to anti-TF Fab'-DACHPt/m, DACHPt/m and oxaliplatin, which is the clinically approved derivative of DACHPt, for 3 h followed by post-incubation for 48 h. The 50% inhibitory concentrations (IC_{50}) of the drugs are summarized in Table 3. The IC_{50} value of DACHPt/m was higher than that of oxaliplatin, as free oxaliplatin is rapidly transported and activated inside the cells, while DACHPt/m are gradually internalized by the endocytosis and sustainedly release cytotoxic Pt complexes [29]. Nevertheless, the IC_{50} value of anti-TF Fab'-DACHPt/m was comparable to that of oxaliplatin, *i.e.* approximately 6-fold lower than that of DACHPt/m. It is worthy of note that, anti-TF Fab' did not show any *in vitro* cytotoxicity against BxPC3 cells under the tested conditions, indicating that the cytotoxicity of anti-TF Fab'-DACHPt/m can be attributed exclusively to the enhanced intracellular delivery of cytotoxic DACHPt. The internalized anti-TF Fab'-DACHPt/m colocalized with late endosomes/lysosomes of BxPC3 (Fig. 5C), which may result in the accelerated release of DACHPt from the anti-TF Fab'-DACHPt/m due to the low pH and high chloride ion concentration of late endosomal and lysosomal compartments [28,29]. Consequently, these results support that, the introduction of anti-TF Fab' on the surface of DACHPt/m may contribute to the substantial improvement of the *in vitro* cytotoxicity through the combination of i) promoted cellular uptake to TF-overexpressing cancer cells (Fig. 5A) and ii) subsequent efficient intracellular delivery of DACHPt *via* endocytosis (Fig. 5C).

3.5. In vivo antitumor efficacy and tumor accumulation of anti-TF Fab'-DACHPt/m

Encouraged by the high *in vitro* cytotoxicity of anti-TF Fab'-DACHPt/m against pancreatic cancer BxPC3 cells, we evaluated the *in vivo* antitumor activity against subcutaneous BxPC3 xenografts. Both DACHPt/m and anti-TF Fab'-DACHPt/m at 3 mg/kg showed enhanced antitumor effect compared to oxaliplatin at 8 mg/kg ($p < 0.001$ and $p < 0.01$, respectively). Particularly, anti-TF Fab'-DACHPt/m suppressed the growth of tumors for approximately 40 days ($p < 0.01$), outperforming DACHPt/m (Fig. 6A). It is worth mentioning that, even though BxPC3 xenografts present characteristics of intractable pancreatic cancer, including poor vascularization, perycite-covered vasculature and thick fibrosis, which impede the access of therapeutic agents [48–50], polymeric micelles with the size smaller than 50 nm showed facilitated penetration and accumulation in this tumor model [35]. Both DACHPt/m and anti-TF Fab'-DACHPt/m showed similar accumulation in tumor tissues (Fig. 6B), which is well-consistent with previously reported antibody-linked nanoparticles [51], indicating that the improved antitumor efficacy of anti-TF Fab'-DACHPt/m did not result from enhanced tumor accumulation. Instead, it is reasonable to assume that the prolonged antitumor efficacy achieved by anti-TF Fab'-DACHPt/m is attributed to the facilitated cellular uptake by TF-targeting (Fig. 5) and the resulting improvement of the cytotoxicity against BxPC3 cells (Table 3). Moreover, at the assessed dosage, neither DACHPt/m nor anti-TF Fab'-DACHPt/m were toxic according to the body weight profile (Fig. 6C). In addition, co-injection of anti-TF Fab' and Mal-DACHPt/m resulted in lower antitumor activity than anti-TF Fab'-DACHPt/m (Fig. 6D; $p < 0.01$), indicating that anti-TF Fab' may not exert any antitumor effect at the applied dose and that the thiol-maleimide conjugation of anti-TF Fab' on the micelles was an effective strategy for enhancing drug delivery.

4. Conclusions

In the present study, we designed and synthesized the DACHPt-incorporated polymeric micelle equipped with anti-human TF-targetable Fab' fragment on their surface, and demonstrated the feasibility of antitumor efficacy against stroma-rich intractable pancreatic tumors. The utilization of maleimide-thiol chemistry allowed the successful preparation of anti-TF Fab'-DACHPt/m with one-to-one tailored conjugation. Compared with DACHPt/m, antigen-recognition ability of anti-TF Fab' facilitated rapid cellular binding and internalization of anti-TF Fab'-DACHPt/m. Enhanced antitumor efficacy of anti-TF Fab'-DACHPt/m without impairing the safety of parent micelles, as at least suggested from the negligible loss in the body weight of treated mice, confirmed the advantages of *in vivo* tumor targeting by immunomicellar system loaded with platinum drugs, which are key drugs for many clinical anticancer therapies, for the first time. This strategy of one-to-one conjugation of Fab' fragment of antibody to polymeric micellar surface by maleimide-thiol coupling is applicable to a broad variety of cargo molecules and antibodies, including clinically approved tumor-directed antibodies, without substantial change in the structure and the size of parent micelles. Hence, it should provide a universality to deliver therapeutic agents into stroma-rich intractable tumors with strict limitation in extravasation of carrier systems, including pancreatic tumor as reported here, and enhance their therapeutic efficacy.

Acknowledgments

The authors thank R. Shiratori and N. Henzan for helping with synthesis experiments, Y. Mochida for micelle characterization, and K. Date for assistance with animal experiments. The authors also thank M. Naito for FCS analysis. This work was supported by the Funding Program for World-Leading Innovative R&D on Science and Technology (FIRST Program) from the Japan Society for the Promotion of Science (JSPS) (KK), Grants-in-Aid for Scientific Research from the Japanese Ministry of Health, Labor, and Welfare (MHLW) (NN, KK), and Center of Innovation Program (COI) from the Ministry of Education, Culture, Sports, Science and Technology (MEXT) (KK). This study was partially supported by Grants-in-Aid for Young Scientists (B; No. 23700526 and No. 25750172 to HC; and A; No. 24689051 to YM), Challenging Exploratory Research (No. 24659584 to YM), Initiative for Accelerating Regulatory Science in Innovative Drug, Medical Device, and Regenerative Medicine (KK), the National Cancer Center Research and Development Fund (YM) and the Health and Labour Sciences Research Grants (Clinical Trial on Development of New Drugs and Medical Devices) (YM).

References

[1] Trail P. Antibody drug conjugates as cancer therapeutics. Antibodies 2013;2:113–29.

[2] Flygare JA, Pillow TH, Aristoff P. Antibody-drug conjugates for the treatment of cancer. Chem Biol Drug Des 2013;81:113–21.
[3] Mullard A. Maturing antibody-drug conjugate pipeline hits 30. Nat Rev Drug Discov 2013;12:329–32.
[4] McDonagh CF, Turcott E, Westendorf L, Webster JB, Alley SC, Kim K, et al. Engineered antibody–drug conjugates with defined sites and stoichiometries of drug attachment. Protein Eng Des Sel 2006;19:299–307.
[5] Shen BQ, Xu K, Liu L, Raab H, Bhakta S, Kenrick M, et al. Conjugation site modulates the in vivo stability and therapeutic activity of antibody-drug conjugates. Nat Biotechnol 2012;30:184–9.
[6] Senter PD, Sievers EL. The discovery and development of brentuximab vedotin for use in relapsed Hodgkin lymphoma and systemic anaplastic large cell lymphoma. Nat Biotechnol 2012;30:631–7.
[7] Hamblett KJ, Senter PD, Chace DF, Sun MM, Lenox J, Cerveny CG, et al. Effects of drug loading on the antitumor activity of a monoclonal antibody drug conjugate. Clin Cancer Res 2004;10:7063–70.
[8] Doronina SO, Toki BE, Torgov MY, Mendelsohn BA, Cerveny CG, Chace DF, et al. Development of potent monoclonal antibody auristatin conjugates for cancer therapy. Nat Biotechnol 2003;21:778–84.
[9] Junutula JR, Raab H, Clark S, Bhakta S, Leipold DD, Weir S, et al. Site-specific conjugation of a cytotoxic drug to an antibody improves the therapeutic index. Nat Biotechnol 2008;26:925–32.
[10] Lewis Phillips GD, Li G, Dugger DL, Crocker LM, Parsons KL, Mai E, et al. Targeting HER2-positive breast cancer with trastuzumab-DM1, an antibody-cytotoxic drug conjugate. Cancer Res 2008;68:9280–90.
[11] LoRusso PM, Weiss D, Guardino E, Girish S, Sliwkowski MX. Trastuzumab emtansine: a unique antibody-drug conjugate in development for human epidermal growth factor receptor 2-positive cancer. Clin Cancer Res 2011;17:6437–47.
[12] Sievers EL, Senter PD. Antibody-drug conjugates in cancer therapy. Annu Rev Med 2013;64:15–29.
[13] Ducry L, Stump B. Antibody-drug conjugates: linking cytotoxic payloads to monoclonal antibodies. Bioconjug Chem 2010;21:5–13.
[14] Wu AM, Senter PD. Arming antibodies: prospects and challenges for immunoconjugates. Nat Biotechnol 2005;23:1137–46.
[15] Yokoyama M, Inoue S, Kataoka K, Yui N, Okano T, Sakurai Y. Molecular design for missile drug: synthesis of adriamycin conjugated with immunoglobulin G using poly(ethylene glycol)-block-poly(aspartic acid) as intermediate carrier. Makromol Chem 1989;190:2041–54.
[16] Aliabadi HM, Lavasanifar A. Polymeric micelles for drug delivery. Expert Opin Drug Deliv 2006;3:139–62.
[17] Kataoka K, Harada A, Nagasaki Y. Block copolymer micelles for drug delivery: design, characterization and biological significance. Adv Drug Deliv Rev 2001;47:113–31.
[18] Nishiyama N, Kataoka K. Current state, achievements, and future prospects of polymeric micelles as nanocarriers for drug and gene delivery. Pharmacol Ther 2006;112:630–48.
[19] Osada K, Christie RJ, Kataoka K. Polymeric micelles from poly(ethylene glycol)-poly(amino acid) block copolymer for drug and gene delivery. J R Soc Interface 2009;6(Suppl. 3):S325–39.
[20] Greish K. Enhanced permeability and retention (EPR) effect for anticancer nanomedicine drug targeting. Methods Mol Biol 2010;624:25–37.
[21] Matsumura Y, Maeda H. A new concept for macromolecular therapeutics in cancer chemotherapy: mechanism of tumoritropic accumulation of proteins and the antitumor agent smancs. Cancer Res 1986;46:6387–92.
[22] Gao Z, Lukyanov AN, Chakilam AR, Torchilin VP. PEG-PE/phosphatidylcholine mixed immunomicelles specifically deliver encapsulated taxol to tumor cells of different origin and promote their efficient killing. J Drug Target 2003;11:87–92.
[23] Torchilin VP, Lukyanov AN, Gao Z, Papahadjopoulos-Sternberg B. Immunomicelles: targeted pharmaceutical carriers for poorly soluble drugs. Proc Natl Acad Sci U S A 2003;100:6039–44.
[24] Noh T, Kook YH, Park C, Youn H, Kim H, Oh ET, et al. Block copolymer micelles conjugated with anti-EGFR antibody for targeted delivery of anticancer drug. J Polym Sci Pol Chem 2008;46:7321–31.
[25] Li W, Zhao H, Qian W, Li H, Zhang L, Ye Z, et al. Chemotherapy for gastric cancer by finely tailoring anti-Her2 anchored dual targeting immunomicelles. Biomaterials 2012;33:5349–62.
[26] Song H, He R, Wang K, Ruan J, Bao C, Li N, et al. Anti-HIF-1alpha antibody-conjugated pluronic triblock copolymers encapsulated with paclitaxel for tumor targeting therapy. Biomaterials 2010;31:2302–12.
[27] Cabral H, Kataoka K. Progress of drug-loaded polymeric micelles into clinical studies. J Control Release 2014;190:465–76.
[28] Cabral H, Nishiyama N, Okazaki S, Koyama H, Kataoka K. Preparation and biological properties of dichloro(1,2-diaminocyclohexane)platinum(II) (DACHPt)-loaded polymeric micelles. J Control Release 2005;101:223–32.
[29] Murakami M, Cabral H, Matsumoto Y, Wu S, Kano MR, Yamori T, et al. Improving drug potency and efficacy by nanocarrier-mediated subcellular targeting. Sci Transl Med 2011;3. 64ra2.
[30] Nitori N, Ino Y, Nakanishi Y, Yamada T, Honda K, Yanagihara K, et al. Prognostic significance of tissue factor in pancreatic ductal adenocarcinoma. Clin Cancer Res 2005;11:2531–9.
[31] van den Berg YW, Osanto S, Reitsma PH, Versteeg HH. The relationship between tissue factor and cancer progression: insights from bench and bedside. Blood 2012;119:924–32.
[32] Cole M, Bromberg M. Tissue factor as a novel target for treatment of breast cancer. Oncologist 2013;18:14–8.
[33] Lorenzet R, Napoleone E, Celi A, Pellegrini G, Di Santo A. Cell-cell interaction and tissue factor expression. Blood Coagul Fibrinolysis 1998;9:S49–59.
[34] Saito Y, Hashimoto Y, Kuroda J-i, Yasunaga M, Koga Y, Takahashi A, et al. The inhibition of pancreatic cancer invasion-metastasis cascade in both cellular signal and blood coagulation cascade of tissue factor by its neutralisation antibody. Eur J Cancer 2011;47:2230–9.
[35] Cabral H, Matsumoto Y, Mizuno K, Chen Q, Murakami M, Kimura M, et al. Accumulation of sub-100 nm polymeric micelles in poorly permeable tumours depends on size. Nat Nanotechnol 2011;6:815–23.
[36] Kano MR, Bae Y, Iwata C, Morishita Y, Yashiro M, Oka M, et al. Improvement of cancer-targeting therapy, using nanocarriers for intractable solid tumors by inhibition of TGF-beta signaling. Proc Natl Acad Sci U S A 2007;104:3460–5.
[37] Miura Y, Takenaka T, Toh K, Wu S, Nishihara H, Kano MR, et al. Cyclic RGD-linked polymeric micelles for targeted delivery of platinum anticancer drugs to glioblastoma through the blood-brain tumor barrier. ACS Nano 2013;7:8583–92.
[38] Cabral H, Nishiyama N, Kataoka K. Optimization of (1,2-diamino-cyclohexane) platinum(II)-loaded polymeric micelles directed to improved tumor targeting and enhanced antitumor activity. J Control Release 2007;121:146–55.
[39] Mochida Y, Cabral H, Miura Y, Albertini F, Fukushima S, Osada K, et al. Bundled assembly of helical nanostructures in polymeric micelles loaded with platinum drugs enhancing therapeutic efficiency against pancreatic tumor. ACS Nano 2014;8:6724–38.
[40] Alley SC, Benjamin DR, Jeffrey SC, Okeley NM, Meyer DL, Sanderson RJ, et al. Contribution of linker stability to the activities of anticancer immunoconjugates. Bioconjug Chem 2008;19:759–65.
[41] Erickson HK, Park PU, Widdison WC, Kovtun YV, Garrett LM, Hoffman K, et al. Antibody-maytansinoid conjugates are activated in targeted cancer cells by lysosomal degradation and linker-dependent intracellular processing. Cancer Res 2006;66:4426–33.
[42] Humphreys DP, Heywood SP, Henry A, Ait-Lhadj L, Antoniw P, Palframan R, et al. Alternative antibody Fab' fragment PEGylation strategies: combination of strong reducing agents, disruption of the interchain disulphide bond and disulphide engineering. Protein Eng Des Sel 2007;20:227–34.
[43] Song HY, Ngai MH, Song ZY, MacAry PA, Hobley J, Lear MJ. Practical synthesis of maleimides and coumarin-linked probes for protein and antibody labelling via reduction of native disulfides. J Org Biomol Chem 2009;7:3400–6.
[44] Thorpe PE, Wallace PM, Knowles PP, Relf MG, Brown AN, Watson GJ, et al. New coupling agents for the synthesis of immunotoxins containing a hindered disulfide bond with improved stability in vivo. Cancer Res 1987;47:5924–31.
[45] Barginear MF, Budman DR. Trastuzumab-DM1: a review of the novel immuno-conjugate for her2-overexpressing breast cancer. Open Breast Cancer J 2009;1:25–30.
[46] Chu TW, Yang J, Kopecek J. Anti-CD20 multivalent HPMA copolymer-Fab' conjugates for the direct induction of apoptosis. Biomaterials 2012;33:7174–81.
[47] Breij EC, de Goeij BE, Verploegen S, Schuurhuis DH, Amirkhosravi A, Francis J, et al. An antibody-drug conjugate that targets tissue factor exhibits potent therapeutic activity against a broad range of solid tumors. Cancer Res 2014;74:1214–26.
[48] Sofuni A, Iijima H, Moriyasu F, Nakayama D, Shimizu M, Nakamura K, et al. Differential diagnosis of pancreatic tumors using ultrasound contrast imaging. J Gastroenterol 2005;40:518–25.
[49] Kano MR, Komuta Y, Iwata C, Oka M, Shirai Y-t, Morishita Y, et al. Comparison of the effects of the kinase inhibitors imatinib, sorafenib, and transforming growth factor-β receptor inhibitor on extravasation of nanoparticles from neovasculature. Cancer Sci 2009;100:173–80.
[50] Dirisala A, Osada K, Chen Q, Tockary TA, Machitani K, Osawa S, et al. Optimized rod length of polyplex micelles for maximizing transfection efficiency and their performance in systemic gene therapy against stroma-rich pancreatic tumors. Biomaterials 2014;35:5359–68.
[51] Kirpotin DB, Drummond DC, Shao Y, Shalaby MR, Hong K, Nielsen UB, et al. Antibody targeting of long-circulating lipidic nanoparticles does not increase tumor localization but does increase internalization in animal models. Cancer Res 2006;66:6732–40.